Readjustment of glacial radiocarbon chronologies by self-consistent three-dimensional ocean circulation modeling

Martin Butzin [a,b,*], Matthias Prange [a], Gerrit Lohmann [a,b]

[a] MARUM–Center for Marine Environmental Sciences, University of Bremen, P.O. Box 330440, D-28334 Bremen, Germany
[b] Alfred Wegener Institute for Polar and Marine Research, P.O. Box 120161, Bussestr. 24, D-27570 Bremerhaven, Germany

ARTICLE INFO

ABSTRACT

A critical problem in radiocarbon dating is the spatial and temporal variability of marine ^{14}C reservoir ages. This is particularly true for the time scale beyond the tree-ring calibration range. Here, we propose a method to assess the evolution of marine reservoir ages during the last deglaciation by numerical modeling. We apply a self-consistent iteration scheme in which existing radiocarbon chronologies can be readjusted by transient, three-dimensional simulations of marine and atmospheric Δ^{14}C. To estimate the uncertainties regarding the ocean ventilation during the last deglaciation, we consider various ocean overturning scenarios which are based on different climatic background states. An example readjusting ^{14}C data from the Caribbean points to marine reservoir ages varying between 200 and 900 a during the last deglaciation. Correspondingly, the readjustment leads to enhanced variability of atmospheric Δ^{14}C by $\pm30‰$, and increases the mysterious drop of atmospheric Δ^{14}C between 17.5 and 14.5 cal ka BP by about 20‰.

1. Introduction

Radiocarbon (^{14}C) dating for the time scale beyond the tree-ring period (i.e. before about 12.5 cal ka BP) mostly relies on cross-dated marine records such as laminated sediments or corals (cf. Chiu et al., 2007; Hughen et al., 2006 and references therein). Atmospheric ^{14}C chronologies derived from marine data have to account for an inherent offset between marine and atmospheric concentrations. For the pre-industrial Holocene, this concentration difference translates into an apparent surface water ^{14}C age (or "marine reservoir age", MRA) of about 400 a in the global mean, ranging from 300 a in the subtropics to up to 1000 years in high latitudes (e.g. Key et al., 2004). The reasons for this offset are different time scales for air-sea exchange, dispersal by ocean mixing and radioactive decay. As the first two processes depend on climate, it can be expected that MRAs for the Last Glacial Maximum (LGM) and the last deglaciation should have differed from Holocene values (e.g. Bard, 1988; Butzin et al., 2005). This is corroborated by observational evidence for considerably higher MRAs during the last deglaciation, at least episodically and for certain regions (e.g. Björck et al., 2003; Bondevik et al., 2006; Cao et al., 2007; Hanslik et al., 2010; Kromer et al., 2004; Sarnthein et al., 2007).

So far, most ^{14}C calibration efforts have not accounted for glacial–interglacial MRA changes. For example, the calibration curves provided by the IntCal group (IntCal09 and Marine09, see Reimer et al., 2009)

adopt a constant MRA value of 405 years for the period 12.5–50 cal ka BP. Here, we make an attempt to assess the evolution of MRAs during the last deglaciation by numerical modeling. We propose an iteration scheme in which existing radiocarbon chronologies can be readjusted by transient simulations of Δ^{14}C. Our approach will be described in the next section. To estimate the uncertainties regarding the ocean circulation during the last deglaciation, we study various forcing scenarios which will be discussed in Section 3. The resulting envelope is a step forward towards more accurate radiocarbon chronologies for the last deglaciation within reasonable uncertainty ranges.

2. Method and model

2.1. General approach

The atmospheric Δ^{14}C history shows a long-term decrease since the LGM which is superimposed by short-term fluctuations. The reason are variations of atmospheric ^{14}C production, as well as climate regime shifts which affect the ^{14}C partitioning between the atmosphere and the ocean, such as glacial–interglacial changes of atmospheric carbon dioxide (CO_2) levels and deep-sea ventilation. It has been shown that all these factors can affect MRAs (e.g. Bard, 1988), which implies that atmospheric Δ^{14}C reconstructions for the LGM and the last deglaciation based on marine data with constant MRA corrections do not capture the real ^{14}C evolution.

In the following discussion we assume that for a given climatic background state, the deglacial radiocarbon transient in the atmosphere is dominated by processes which (approximately) follow zero- or first-order kinetics, i.e. by cosmogenic production, air-sea exchange and

* Corresponding author. Tel./fax: +49 421 21 86 54 55.
E-mail address: mbutzin@marum.de (M. Butzin).

radioactive decay. In this case the progression of MRAs can be approximated by an iterative, self-consistent calculation scheme. The basic idea is to infer atmospheric Δ^{14}C and MRAs from marine reconstructions by back and forth model calculations of ^{14}C in atmosphere and ocean. We do not consider the effect of deglacial vegetation growth on MRAs because the mean residence time of ^{14}C in modern terrestrial biota is much shorter than in the ocean (e.g. Siegenthaler and Joos, 1992).

Our iteration starts with a prescribed atmospheric radiocarbon chronology $^{14}C_{atm}^{(0)}$ which has been derived from marine observations according to $^{14}C_{atm}^{(0)} = {}^{14}C_{mar}^{obs} exp(\lambda\tau_0)$, where $^{14}C_{mar}^{obs}$ is the underlying marine record at a given location and our iteration target, τ_0 is an assumed MRA correction, and $\lambda = 1.2096\times10^{-4}$ a^{-1} is the decay constant of radiocarbon (Godwin, 1962). We employ an ocean model to diagnose the corresponding evolution of ^{14}C concentrations and MRAs in surface water. Ideally, model concentrations $^{14}C_{mar}^{mod}$ and observations $^{14}C_{mar}^{obs}$ should be the same. If there are significant differences, we assume that the atmospheric ^{14}C input curve should be corrected. For this purpose we reestimate $^{14}C_{atm}^{(1)} = {}^{14}C_{mar}^{obs} exp(\lambda\tau_1)$, where $^{14}C_{atm}^{(1)}$ is the readjusted atmospheric radiocarbon history and $\tau_1 = \lambda^{-1} ln({}^{14}C_{atm}^{(0)}/{}^{14}C_{mar}^{mod(1)})$ the MRA evolution diagnosed during the first model run. Then the model calculations are repeated, now taking $^{14}C_{atm}^{(1)}$ as the new input curve and diagnosing a second time series of surface water concentrations and reservoir ages τ_2. As the inertia of the marine ^{14}C cycle may cause leads and lags in the surface water history, it is possible that the new model surface water concentrations are not yet consistent with the observations. If this is the case, we readjust $^{14}C_{atm}^{(1)}$ to give $^{14}C_{atm}^{(2)} = {}^{14}C_{mar}^{obs} exp(\lambda\tau_2)$, and we have to go for a further iteration loop, and so on. The iteration stops when the modeled surface water concentrations approach $^{14}C_{mar}^{obs}$ which implies that MRAs and the derived atmospheric Δ^{14}C chronology are consistent with the marine radiocarbon record. Our criterion of convergence is $\langle\Delta\Delta^{14}C\rangle < 2‰$, where $\langle\Delta\Delta^{14}C\rangle$ is the annual root-mean-square difference between modeled and measured marine Δ^{14}C. This is equivalent to MRA uncertainties of less than 20 years. Four iterations were sufficient to achieve convergence in each simulation presented below.

A critical variable in our approach is the intensity of the glacial and deglacial ocean ventilation which is governed by the climatic background state and is still subject of discussions (e.g. Lynch-Stieglitz et al., 2007; Meland et al., 2008; Otto-Bliesner et al., 2007). To assess this complication, we consider various ocean overturning scenarios which give an estimate of the uncertainty range of the readjusted ^{14}C curves, and which will be discussed in further detail below.

2.2. Model description and experimental design

Our investigations are carried out using a three-dimensional ocean circulation model which is connected with an atmospheric radiocarbon reservoir. We employ an improved version of the Hamburg LSG ocean circulation model (Maier-Reimer et al., 1993; Prange et al., 2003). Major improvements are a third-order transport scheme for tracers (Prange et al., 2003; Schäfer-Neth and Paul, 2001) as well as an overflow parametrization for the bottom boundary layer (Lohmann, 1998). The setup is described in further detail by Butzin et al. (2005). The ocean model has an effective horizontal resolution of 3.5° on an Arakawa-E grid and 22 levels. It is forced with monthly fields of wind stress, surface air temperature and freshwater flux derived in simulations using the atmosphere general circulation model ECHAM3/T42, which by itself is forced with prescribed values of insolation, greenhouse gases, ice-sheet and sea-ice cover as well as sea surface temperatures (SSTs; described by Lohmann and Lorenz, 2000; Prange et al., 2004). We consider four forcing cases. Scenario PD employs present-day climate forcing fields, and the resulting ocean circulation is also regarded as a surrogate for interstadial climate conditions such as during the Bølling-Allerød (BA) warm interval. Scenario GS (Butzin et al., 2005) employs boundary conditions for the LGM. The atmospheric forcing in this scenario employs SSTs of the

GLAMAP 2000 reconstruction for the Atlantic (see Sarnthein et al., 2003 and references therein) in the globally extended version of Paul and Schäfer-Neth (2003). A modified freshwater balance in the Southern Ocean mimics enhanced northward sea ice export as suggested by LGM modeling studies (e.g. Shin et al., 2003).

Compared to case PD, the meridional overturning circulation (MOC) shallows to a depth above about 2 km and weakens by about 40% in the North Atlantic while formation of deep and bottom water masses in the Southern Ocean is enhanced (Fig. 1). As a consequence, the modeled abyssal glacial Atlantic is depleted in ^{14}C, very cold and very saline (cf. Fig. 6d in Butzin et al., 2005). This scenario is line with marine ^{14}C records and with other proxy data evidence for the LGM and the last deglaciation (see Lynch-Stieglitz et al., 2007 for a review).

In addition to these steady-state scenarios (presented in Section 3.3.1), experiments HPD and HGS investigate the effect of an abrupt MOC perturbation associated with meltwater discharge during Heinrich event 1 (H1). Atmospheric forcing in the transient simulations is according to scenarios PD and GS, but our surface heat flux parametrization permits free adjustment of SSTs in response to ocean circulation changes (Prange et al., 2003, 2004). The meltwater perturbation experiments will be the topic of Section 3.3.2.

Radiocarbon is modeled as Δ^{14}C similar to Toggweiler et al. (1989). The model is calibrated to capture the prebomb distribution
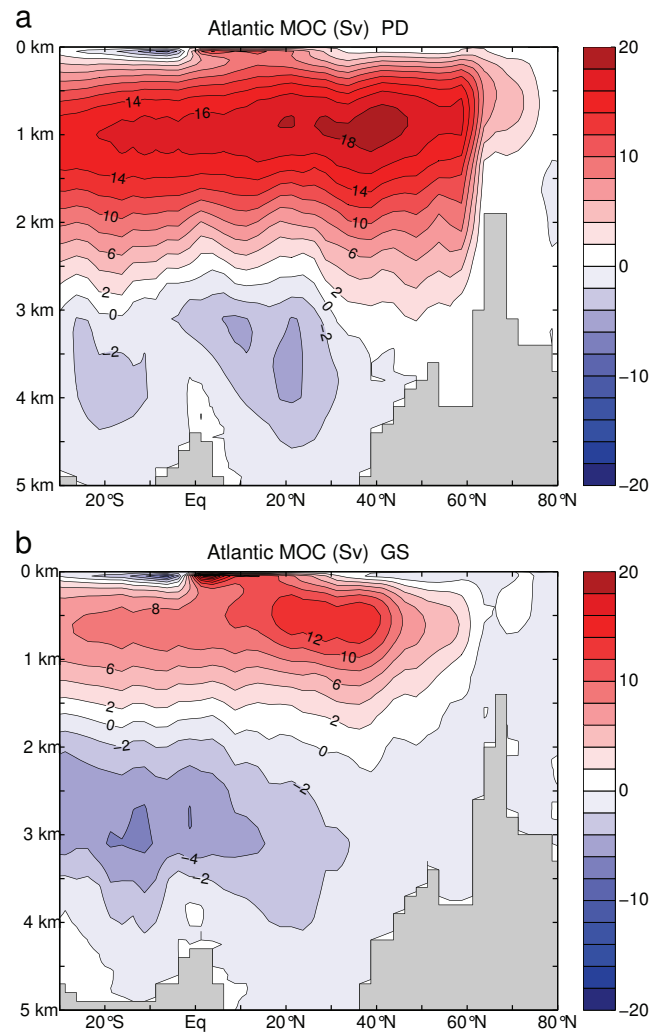

Fig. 1. Meridional overturning circulation (Sv, $1\,Sv = 1\times10^6\,m^3/s$) in the Atlantic. a) Scenario PD, b) scenario GS.

of marine Δ^{14}C as well as glacial top-bottom ^{14}C age differences according to corals and foraminifera (Butzin et al., 2005). We employ an air-sea exchange formulation which allows for various climatic boundary conditions. Gas transfer velocities are updated according to recent estimates by Sweeney et al. (2007). This leads to systematically higher MRAs than in our previous study (Butzin et al., 2005) and is further discussed in the Appendix A.

3. Results

3.1. Control run and model spinup

The starting point for our considerations are quasi steady state conditions typical for 25 cal ka BP, which were obtained in spinup integrations (over 10,000 years) using fixed atmospheric background values of Δ^{14}C = 520‰ (Reimer et al., 2009) and CO_2 = 185 ppmv (Fischer et al., 1999). At the end of the model spinup, the MRA averaged over of the ice-free areas of the global ocean is ~830 a for PD climate forcing. In scenario GS the average MRA of the ice-free seas is ~940 a. In the following discussion we will focus on the Caribbean Sea, as a recent ^{14}C reconstruction over the last 50,000 years contributing to IntCal09 is based on non-varved marine sediment data from the Cariaco Basin off Venezuela (~10.7°N, 65.2°W; Hughen et al., 2006). For this location the MRAs at the end of the model spinup are about 600 a for PD and 730 a for GS, respectively. A control integration using PD climate forcing and preindustrial values for atmospheric Δ^{14}C (0‰) and CO_2 (280 ppmv) yields for the Cariaco Basin a MRA of about 350 a, which is in the range of reconstructions for the beginning of the 20th century (312–361 a; Hughen et al., 2004; Guilderson et al., 2005; see also Fig. S1 in the Appendix A).

3.2. Sensitivity to transient CO_2 levels

Between 18 and 14 cal ka BP atmospheric CO_2 concentrations increased by about 25%. To explore the effect on MRAs, we run sensitivity simulations with transient CO_2 concentrations (according to Monnin et al., 2001; revised age control by Köhler et al., 2005) while atmospheric Δ^{14}C is kept constant at 520‰. The results are shown in Fig. 2. For the PD ocean circulation field, Caribbean reservoir ages decrease from ~580 to 440 a. Using ocean circulation field GS, we arrive at a decrease from ~700 to 530 a. In both cases, there is a rapid MRA response to increasing atmospheric CO_2 levels which enhance the air-sea gas exchange and hence oceanic uptake of radiocarbon. Global-mean MRAs are higher than Caribbean ages but the response
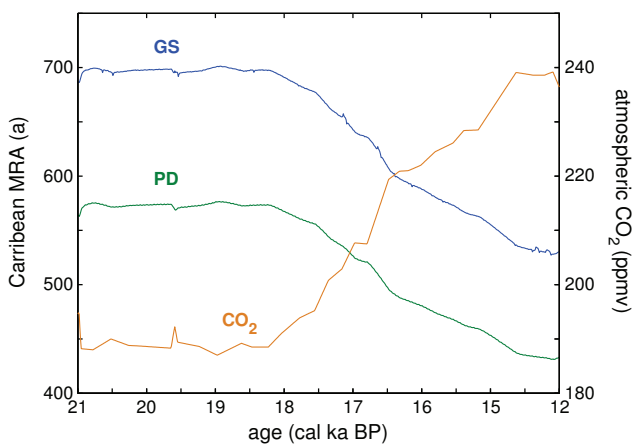

Fig. 2. Response of marine ^{14}C reservoir ages (MRA) in the Caribbean Sea to increasing atmospheric CO_2 concentrations. PD: MRA response assuming present-day / interstadial ocean ventilation, GS: MRA response assuming glacial ocean ventilation. Shown are the results for 21–14 cal ka BP.

to CO_2 variations is of similar magnitude (PD: from 840 to 680 a, GS: from 940 to 780 a; not shown). In reality the CO_2 effect on MRAs is superimposed by the effect of atmospheric Δ^{14}C variations (e.g. due to cosmogenic production changes). In the following considerations these variations are taken into account.

3.3. Readjustment of a ^{14}C chronology

To demonstrate the readjustment method, we consider an atmospheric ^{14}C chronology for 14–25 cal ka BP derived from a marine sediment record in the Cariaco Basin (Hughen et al., 2006), which is also included in the IntCal09 curve. In this example, the original reservoir age correction τ_0 is 420 a. To account for observational uncertainties, the underlying marine radiocarbon data $^{14}C_{mar}^{obs}$ have been smoothed using a 200 year running average (tentatively assumed on the basis of the uncertainties reported by Hughen et al., 2006; see Section 4 for further discussion).

During the model runs, atmospheric CO_2 is kept constant at 185 ppmv over the first 4000 years (i.e., for 25–21 cal ka BP), while concentrations for 21–14 cal ka BP are variable according to the Antarctic Dome C ice core record (Monnin et al., 2001; revised age control by Köhler et al., 2005). We evaluate model results for the Caribbean Sea off the Venezuelan coast in the top layer between 0 and 50 m depth, corresponding to the location and the typical habitat depth where most foraminifera were sampled by Hughen et al. (2006). We focus on 21–14 cal ka BP and do not consider the results for 25–21 cal ka BP which may reflect an initial transient response of the model to the imposed fluctuating atmospheric ^{14}C values.

3.3.1. Steady-state ocean circulation

At the beginning, $\langle\Delta\Delta^{14}C\rangle$ is 16‰ for PD and 18‰ for GS, respectively. After four readjustments $\langle\Delta\Delta^{14}C\rangle$ is smaller than 2 (1.6‰ for PD and 1.9‰ for GS, respectively; Fig. 3 illustrates the convergence of solutions). Accordingly, Caribbean MRAs relax from $\tau_0 = 420$ a to τ_4~210–740 a for PD and τ_4~260–890 a for GS, respectively (Fig. 4). Readjustment of $\Delta^{14}C_{atm}^{(0)}$ by means of $\tau_{1...4}$ increases atmospheric values prior to ~16.3 cal ka BP (when CO_2 concentrations are less than 221 ppmv), as can be seen in Fig. 5. The opposite is found between ~16.3–14.0 cal ka BP. Atmospheric values for GS are always higher than for PD as a consequence of the weaker glacial ocean ventilation.

3.3.2. Abrupt shutdown of the meridional overturning circulation

Sediment records of ^{231}Pa/^{230}Th activities suggest a substantial weakening of the Atlantic MOC between 17.5 and 15 cal ka BP associated with H1 (Gherardi et al., 2005, 2009; McManus et al., 2004; see also Burke et al., 2011; Peacock, 2010 for critical assessments). To investigate the effect of these abrupt MOC reductions on the deglacial radiocarbon chronology, we additionally consider simulations with a perturbed freshwater balance in the North Atlantic between 40° and 50°N. At runtimes equivalent to 17.5–15 cal ka BP, we inject freshwater at a rather high rate of 0.5 Sv in order to achieve an abrupt and complete MOC shutdown. The MOC response is shown in Fig. 6. The freshwater hosing experiments HPD and HGS build upon $\Delta^{14}C_{atm}^{(4)}$ of constant-MOC scenarios PD and GS and are repeated another four times. After that, $\langle\Delta\Delta^{14}C\rangle$ amounts to 1.3‰ for both experiments HPD and HGS, respectively; see also Fig. 7.

Caribbean MRAs initially drop by up to 200 a in HPD and 230 a in HGS, respectively, compared to the constant-MOC results (Fig. 4). After about 300 a of freshwater hosing Caribbean MRAs start to increase again. In experiment HPD the increase is rather continuous, τ_4^{HPD} exceeds τ_4^{PD} after 1600 a (= 15.9 cal ka BP), and at the end τ_4^{HPD} is by 70 a higher than τ_4^{PD}. In case HGS τ_4^{HGS} stabilizes after 1700 a (= 15.8 cal ka BP) at values which are about 50 a lower than τ_4^{GS}. When the freshwater hosing is switched off τ_4^{HGS} increases by more than 100 a within a few decades, and at the end τ_4^{HGS} is about 40 a higher than τ_4^{GS}.
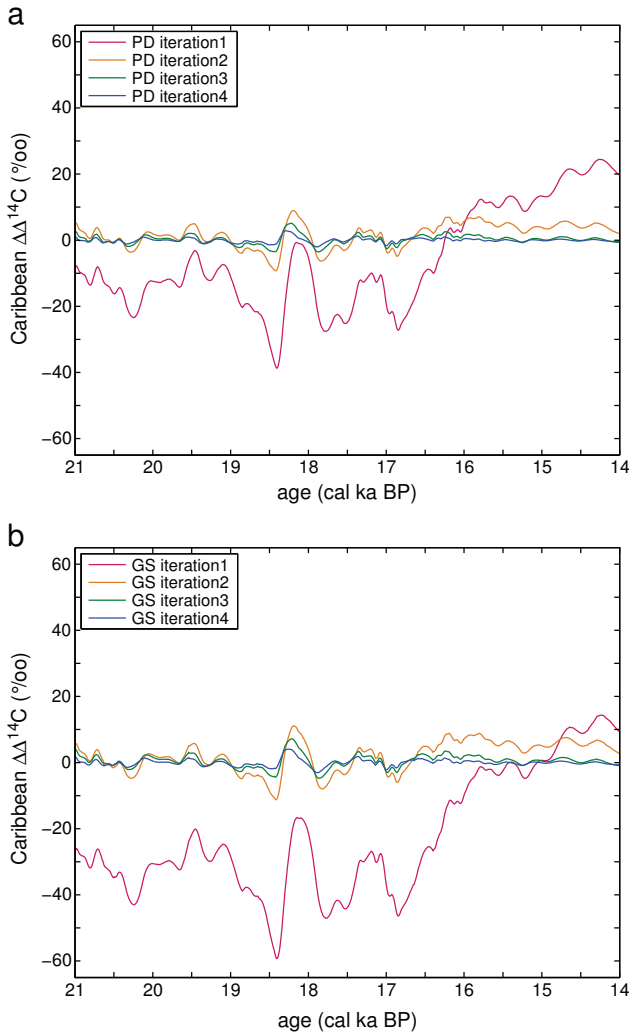
a

b

Fig. 3. Convergence of modeled $\Delta^{14}C_{mar}^{mod}$ during the iterations, shown is the difference $\Delta\Delta^{14}C$ to observations. a) Ocean ventilation scenario PD, b) ocean ventilation scenario GS.

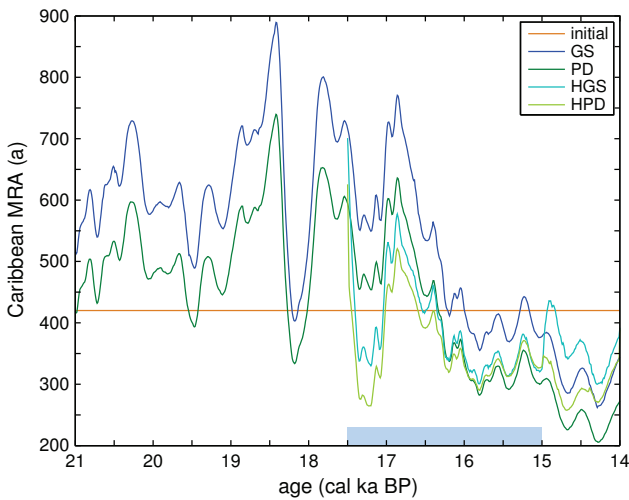**Fig. 4.** Temporal evolution of readjusted marine ^{14}C reservoir ages (MRA) in the Caribbean, shown are results after four iterations of each MOC scenario. The horizontal blue bar indicates the period of freshwater hosing in transient-MOC simulations HPD and HGS (hosing rate = 0.5 Sv).

Fig. 5. Temporal evolution of readjusted atmospheric ^{14}C chronologies, shown are results after four iterations of each MOC scenario. The horizontal blue bar indicates the period of freshwater hosing in transient-MOC simulations HPD and HGS (hosing rate = 0.5 Sv).
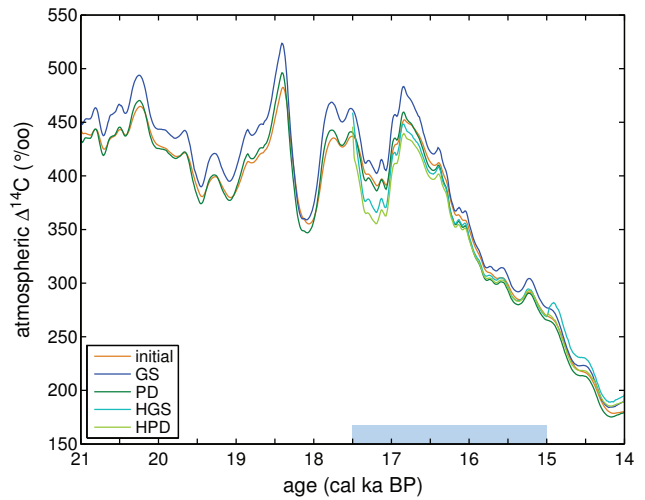
The evolution of τ_4^{HPD} and τ_4^{HGS} leads to an abrupt initial drop of atmospheric Δ^{14}C curves compared to the unperturbed cases which is shown in Fig. 5. In scenario HPD atmospheric values remain smaller than $\Delta^{14}C_{atm}^{PD(4)}$ between 17.5 and 15.9 cal ka BP but become elevated in younger periods. Experiment HGS shows $\Delta^{14}C_{atm}^{HGS(4)}$ running below $\Delta^{14}C_{atm}^{GS(4)}$ during the entire period of freshwater hosing followed by an abrupt increase afterwards.

4. Discussion

To capture the uncertainty caused by climate and ocean ventilation variability during the last deglaciation, we combine the results of all scenarios, mimicking the termination from the LGM via H1 to the BA interstadial. By considering the extreme outcomes we obtain estimates of upper and lower bounds for the readjusted MRA and atmospheric Δ^{14}C curves.

Fig. 8 shows the resulting envelope of MRAs. The long-term decrease caused by rising deglacial CO_2 levels is superimposed by millennial-scale variability. We conjecture that real MRAs approached the upper bound of the age envelope in times prior to H1 (according
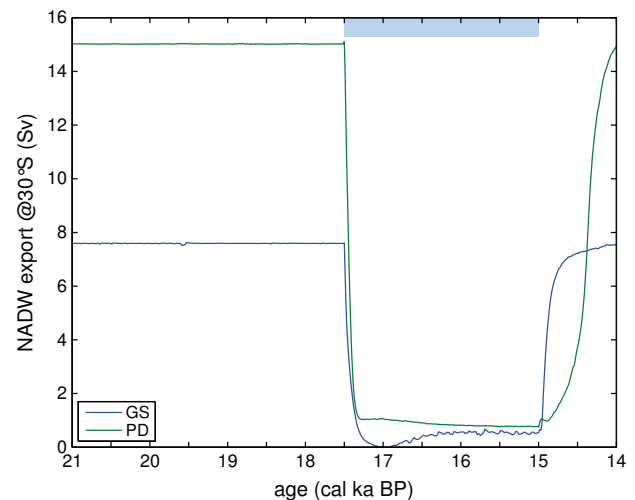

Fig. 6. MOC response to freshwater hosing, shown is the volume transport of North Atlantic Deep Water in the South Atlantic at 30S (in Sv, 1 Sv = 1 × 10^6 m^3/s). The horizontal blue bar indicates the period of freshwater hosing (hosing rate = 0.5 Sv).

Fig. 8. Envelope of marine ^{14}C reservoir ages (MRA) spanned by the self-consistent results of scenarios PD, GS, HPD, and HGS. The sandy line marks the original MRA correction by Hughen et al. (2006).

17.5 and 14.5 cal ka BP discussed by Broecker and Barker (2007) by about 20‰.

Previous modeling sensitivity studies indicated that atmospheric Δ^{14}C increased when the Atlantic MOC was shut down (e.g. Butzin et al., 2005; Ritz et al., 2008; Singarayer et al., 2008). The initial drop of atmospheric Δ^{14}C in meltwater simulations HPD and HGS is consistent with these results. In the previous studies it was necessary to explicitly prescribe a cosmogenic production rate which was kept constant during the MOC perturbation. When the readjustment method is applied to a virtual marine record which was produced in such a simulation (Butzin et al., 2005) it reproduces the positive atmospheric ^{14}C excursion seen before (~30‰). This demonstrates that the approach works independently of ^{14}C production assumptions. The atmospheric Δ^{14}C decline during H1 according to our meltwater simulations is compatible with a modest, temporary ^{14}C production decrease of 15–25% (Fig. S4). However, this should not be mistaken for a statement on the real ^{14}C production history but it is an indication that our MOC perturbation scenarios are rather extreme, providing conservative uncertainty estimates.
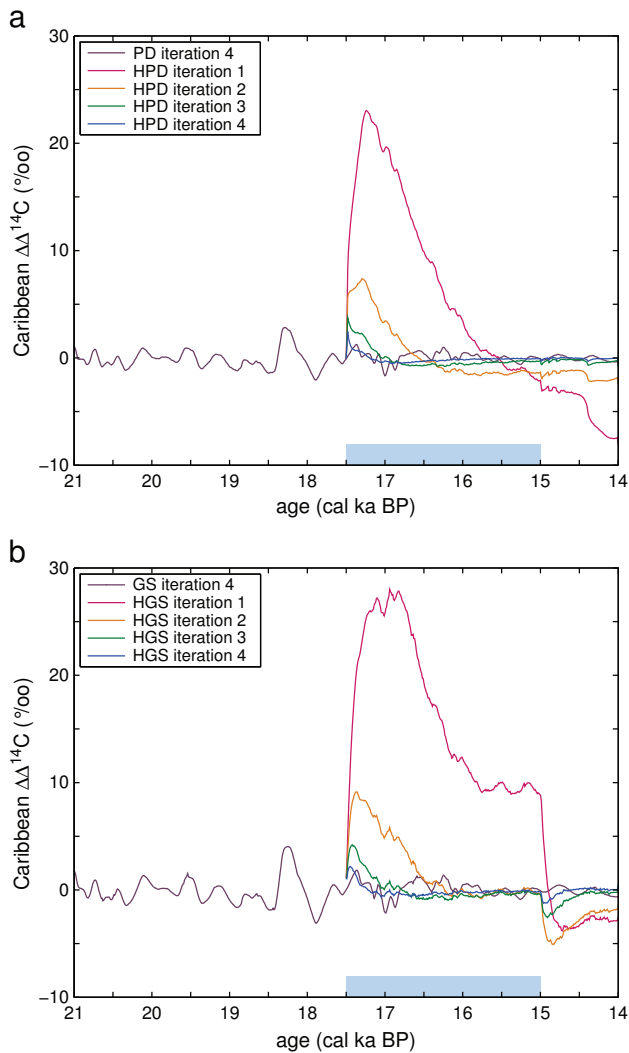

Fig. 7. Convergence of modeled $\Delta^{14}C_{mar}^{mod}$ during the iterations with freshwater hosing, shown is the difference $\Delta\Delta^{14}$C to observations. a) Hosing scenario HPD, b) scenario HGS. The horizontal blue bar indicates the period of freshwater hosing (hosing rate = 0.5 Sv).

to 'glacial' MOC scenario GS). Furthermore, our freshwater-hosing experiments suggest that, if the Atlantic MOC was completely shut down during H1, Caribbean MRAs may have declined to the lower bound of the age envelope approaching almost modern values. Fig. 8 also indicates that the MRA uncertainty due to glacial–interglacial ocean ventilation changes is in the range of 50–150 a except for the early phase of H1 (17.5–16.5 cal ka BP) when the uncertainty increases up to 300 a. A drop in Caribbean MRA has also been found in other modeling studies with freshwater hosing in the North Atlantic (e.g. Ritz et al., 2008; Singarayer et al., 2008).

Analogous considerations apply to the reconstruction of atmospheric radiocarbon concentrations. At a given time, the climatic uncertainty of atmospheric Δ^{14}C is mostly in the range of 10–25‰ (cf. Fig. 9), except for the onset of H1 when the uncertainty range increases to ~50‰. Compared to the original curve, the Δ^{14}C envelope is up to ~80‰ higher for ~21.0–18.3 and 18.0–17.5 cal ka BP. During the first centuries of H1 (until 17.0 cal ka BP) the original Δ^{14}C reconstruction lies within the uncertainty range of the envelope. The atmospheric envelope runs below the original Δ^{14}C curve between ~16.4 and 14 cal ka BP. This implies that our readjustment increases the mysterious drop in atmospheric radiocarbon concentrations between
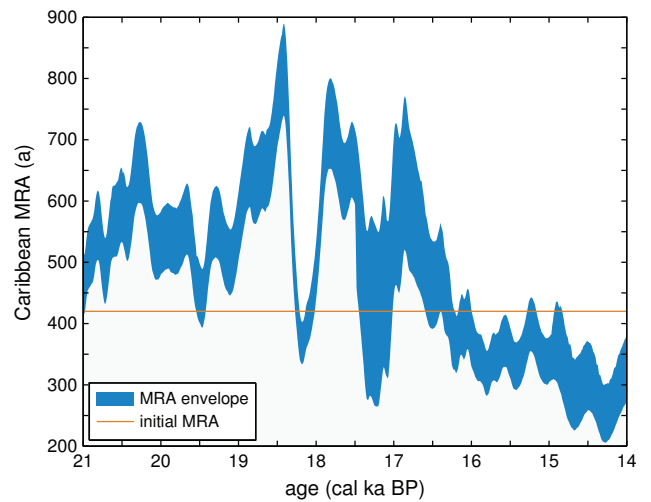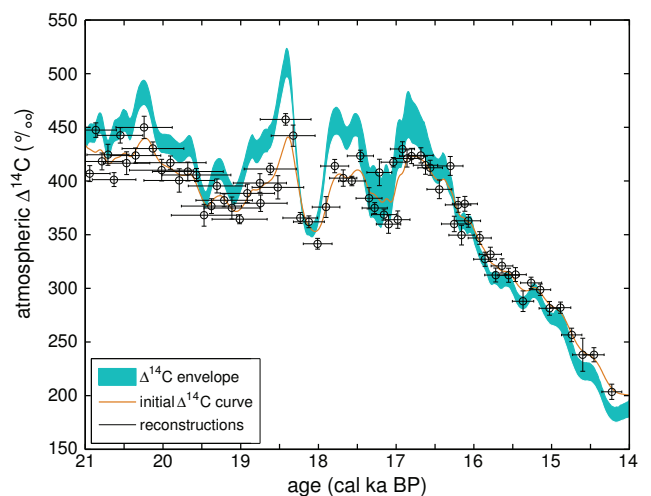

Fig. 9. Envelope of atmospheric ^{14}C chronologies spanned by self-consistent results of scenarios PD, GS, HPD, and HGS. The sandy line marks the input Δ^{14}C chronology adapted from Hughen et al. (2006), dots with errorbars are measurements by Hughen et al. (2006) with a constant MRA correction of 420 a.

A closer inspection of the atmospheric $\Delta^{14}C$ histories indicates that short-term fluctuations already existing in the marine observational record (and iteration target) $^{14}C_{mar}^{obs}$ are amplified by our method. This is caused by the isotopic inertia of the ocean which implicates that ^{14}C concentration changes of surface water lag behind atmospheric concentration changes. During the iterations atmospheric ^{14}C is prescribed. If the model ocean experiences an atmospheric ^{14}C excursion which is sufficiently fast and high (such as around 18.5 ka BP), the sea surface will become isotopically depleted with respect to the atmosphere, and diagnosed MRAs will increase. As a consequence, the corrected atmospheric ^{14}C to be used in the following iteration step further increases. Conversely, a significant drop in atmospheric ^{14}C (such as around 18 ka BP) translates into an isotopically enriched sea surface. This leads to decreasing MRAs which pull atmospheric ^{14}C further downward. The amplification of atmospheric fluctuations is large after the first iteration and decreases with the convergence of $^{14}C_{mar}^{mod}$ and $^{14}C_{mar}^{obs}$, as can be inferred from Figs. 3 and 7. In principle, the isotopic inertia of the ocean depends on the time scale of deep sea ventilation. For this reason the amplitude of atmospheric ^{14}C fluctuations around 18.5–18 ka BP is more pronounced for scenario GS (featuring a sluggish MOC) than for PD. The isotopic feedback also depends on our model's capabilities to respond to transient tracer boundary conditions which may be different in other models (see Orr et al., 2001, for a discussion of the uptake of anthropogenic ^{14}C by different models; note that the LSG model mentioned there is different to our version). Simulations aiming at an unsmoothed iteration target $^{14}C_{mar}^{obs}$ yielded noisier results (not shown). We suspect that such fluctuations are artificial because the error bars reported by Hughen et al. (2006) suggest that most of the short-term variability in $^{14}C_{mar}^{obs}$ can be attributed to data uncertainties. This is the motivation for our initial smoothing of $^{14}C_{mar}^{obs}$ because our approach does not directly incorporate observational uncertainties (different to inverse/adjoint methods such as discussed by Wunsch and Heimbach, 2007). Short-term fluctuations can be further reduced if the model results are additionally smoothed, e.g. after each iteration (not shown), but in this case the readjustment would not be rigorously self-consistent. The centennial to millennial-scale features of our results such as the increased $\Delta^{14}C$ drop between 17.5 and 14.5 cal ka BP are robust and largely independent of the degree of data smoothing.

Scattered reconstructions of strongly depleted ^{14}C values at intermediate depths during H1 have been interpreted with enhanced formation of Antarctic Intermediate Water (AAIW), spreading the isotopic signature of a hypothetical, isolated reservoir from the abyssal Pacific into the Northern Hemisphere (Bryan et al., 2010; Marchitto et al., 2007; Stott et al., 2009; Thornalley et al., 2011). These findings give rise to speculations about an alternative MOC scenario for H1 in which the Cariaco Basin was rather bathed in ^{14}C-depleted AAIW than in a stagnant layer of northern waters. In this case Caribbean MRAs and hence atmospheric $\Delta^{14}C$ would increase during H1. This scenario is not captured by our simulations. However, the reconstructions have been discussed controversially (see Cléroux et al., 2011; De Pol-Holz et al., 2010; Hain et al., 2011; Magana et al., 2010; Mangini et al., 2010; Rose et al., 2010; Sortor and Lund, 2011). Moreover, a prerequisite for this hypothesis is a strongly depleted abyssal ^{14}C reservoir. We do not find such a reservoir in our glacial simulations, and its existence has not been confirmed by observations either (e.g. Broecker and Clark, 2010).

While the simulations were evaluated at model coordinates close to the reconstruction site, our model is not designed for regional studies. The Cariaco Basin is a depression on the continental margin which is about 160 km long, 70 km wide and 1400 m deep, and water exchange with the tropical Atlantic is restricted by sills which are shallower than about 150 m (e.g. Muller-Karger et al., 2004 and references therein). On the other hand, the horizontal model resolution in the Caribbean is more than 300 km. This implies that the model cannot resolve the Cariaco Basin and that the model results may rather reflect conditions typical for the adjacent Caribbean Sea.

Our findings (as well as the results by Hughen et al., 2006) are based on the debatable assumption that atmospheric radiocarbon chronologies derived from a single marine record are representative for the global atmospheric ^{14}C transient. To validate this upscaling approach (which is beyond the scope of this paper) and to rule out local artifacts caused by specific oceanographic settings (which are closely related to the above-mentioned resolution issue), future readjustment efforts should consider further locations with comprehensive glacial–deglacial marine ^{14}C records (e.g. Bard et al., 2004; Chiu et al., 2007; Cutler et al., 2004; Rose et al., 2010 and further references therein).

The initial conditions of our model calculations were defined in steady-state spinup integrations while it is known that neither atmospheric ^{14}C nor climatic conditions were constant prior to the LGM (e.g. Grootes et al., 1993; Hughen et al., 2006). In this pilot study focusing on the last deglaciation, we attempted to overcome this initial value problem by starting from 25 cal ka BP and ignoring the results for 25–21 cal ka BP. An analogous procedure could be applied in investigations extending further back in time. Such studies should also consider further ocean ventilation scenarios to capture the climate variability prior to the LGM. Moreover, future studies could consider different deglacial scenarios including an even abrupter onset of the BA (e.g. Knorr and Lohmann, 2007). The systematic uncertainties could also be narrowed down by ensemble and model intercomparison runs.

5. Conclusions

Our results indicate that current radiocarbon chronologies for the last deglaciation are not self-consistent with their underlying assumption of invariant marine reservoir ages. We have demonstrated that such inconsistencies and their significant effects on ^{14}C calibration curves may be mitigated by iterative modeling. By considering various MOC scenarios according to different climatic background conditions, we sought to estimate the uncertainties which are due to the difficulties in reconstructing the past ocean ventilation. An example from the Caribbean suggests that marine reservoir ages varied between 200 and 900 a during the last deglaciation, leading to enhanced variability of atmospheric $\Delta^{14}C$ by ± 30‰. This may have increased the mysterious drop of atmospheric concentrations between 17.5 and 14.5 cal ka BP by about 20‰.

The outcomes are a step towards more accurate radiocarbon chronologies for the last deglaciation. Our approach is complementary to statistical methods devised for the estimation of ^{14}C calibration curves (e.g. Buck and Blackwell, 2004; Heaton et al., 2009). Although the readjustment approach could be adapted to box models, only three-dimensional models are able to capture the spatial variability of observations. In this respect it is important to note that our model was not designed for regional studies. We recommend that similar investigations in future calibration or reconstruction efforts should be carried out at higher spatial resolution and covering a longer period of time. Such studies should also comprise further locations with glacial–deglacial marine ^{14}C records.

Appendix A. Supplementary data

Supplementary data to this article can be found online at doi:10.1016/j.epsl.2011.11.046.

References

Bard, E., 1988. Correction of accelerator mass spectrometry ^{14}C ages measured on planktonic foraminifera: Paleoceanographic implications. Paleoceanography 3, 635–645.

Bard, E., Ménot-Combes, G., Rostek, F., 2004. Present status of radiocarbon calibration and comparison records based on Polynesian corals and Iberian margin sediments. Radiocarbon 46, 1189–1202.

Björck, S., Koç, N., Skog, G., 2003. Consistently large marine reservoir ages in the Norwegian Sea during the Last Deglaciation. Quat. Sci. Rev. 22, 429–435.

Bondevik, S., Mangerud, J., Birks, H.H., Gulliksen, S., Reimer, P., 2006. Changes in North Atlantic radiocarbon reservoir ages during the Allerød and Younger Dryas. Science 312, 1514–1517.

Broecker, W.S., Barker, S., 2007. A 190‰ drop in atmosphere's Δ^{14}C during the "Mystery Interval" (17.5 to 14.5 kyr). Earth Planet. Sci. Lett. 256, 90–99.

Broecker, W.S., Clark, E., 2010. Search for a glacial-age ^{14}C-depleted ocean reservoir. Geophys. Res. Lett. 37, L13606.

Bryan, S.P., Marchitto, T.M., Lehman, S.J., 2010. The release of ^{14}C-depleted carbon from the deep ocean during the last deglaciation: Evidence from the Arabian Sea. Earth Planet. Sci. Lett. 298, 244–254.

Buck, C.E., Blackwell, P.G., 2004. Formal statistical models for estimating radiocarbon calibration curves. Radiocarbon 46, 1093–1102.

Burke, A., Marchal, O., Bradtmiller, L.I., McManus, J.F., François, R., 2011. Application of an inverse method to interpret ^{231}Pa/^{230}Th observations from marine sediments. Paleoceanography 26, PA1212.

Butzin, M., Prange, M., Lohmann, G., 2005. Radiocarbon simulations for the glacial ocean: The effects of wind stress, Southern Ocean sea ice and Heinrich events. Earth Planet. Sci. Lett. 235, 45–61.

Cao, L., Fairbanks, R.G., Mortlock, R.A., Risk, M.J., 2007. Radiocarbon reservoir age of high latitude North Atlantic surface water during the last deglacial. Quat. Sci. Rev. 26, 732–742.

Chiu, T.-C., Fairbanks, R.G., Cao, L., Mortlock, R.A., 2007. Analysis of the atmospheric ^{14}C record spanning the past 50,000 years derived from high-precision ^{230}Th/^{234}U/^{238}U, ^{231}Pa/^{235}U and ^{14}C dates on fossil corals. Quat. Sci. Rev. 26, 18–36.

Cléroux, C., deMenocal, P., Guilderson, T., 2011. Deglacial radiocarbon history of tropical Atlantic thermocline waters: absence of CO_2 reservoir purging signal. Quat. Sci. Rev. 30, 1875–1882.

Cutler, K.B., Gray, S.C., Burr, G.S., Edwards, R.L., Taylor, F.W., Cabioch, G., Beck, J.W., Cheng, H., Moore, J., 2004. Radiocarbon calibration and comparison to 50 kyr BP with paired ^{14}C and ^{230}Th dating of corals from Vanuatu and Papua New Guinea. Radiocarbon 46, 1127–1160.

De Pol-Holz, R., Keigwin, L., Southon, J., Hebbeln, D., Mohtadi, M., 2010. No signature of abyssal carbon in intermediate waters off Chile during deglaciation. Nat. Geosci. 3, 192–195.

Fischer, H., Wahlen, M., Smith, J., Mastroianni, D., Deck, B., 1999. Ice core records of atmospheric CO_2 around the last three glacial terminations. Science 283, 1712–1714.

Gherardi, J.M., Labeyrie, L., McManus, J.F., François, R., Skinner, L.C., Cortijo, E., 2005. Evidence from the Northeastern Atlantic basin for variability in the rate of the meridional overturning circulation through the last deglaciation. Earth Planet. Sci. Lett. 240, 710–723.

Gherardi, J.-M., Labeyrie, L., Nave, S., François, R., McManus, J.F., Cortijo, E., 2009. Glacial-interglacial circulation changes inferred from ^{231}Pa/^{230}Th ratios sedimentary record in the North Atlantic region. Paleoceanography 24, PA2204.

Godwin, H., 1962. Half-life of radiocarbon. Nature 195, 984.

Grootes, P.M., Stuiver, M., White, J.W.C., Johnsen, S., Jouzel, J., 1993. Comparison of oxygen isotope records from the GISP2 and GRIP ice cores. Nature 366, 552–554.

Guilderson, T.P., Cole, J.E., Southon, J.R., 2005. Pre-bomb Δ^{14}C variability and the Suess effect in Cariaco Basin surface waters as recorded in hermatypic corals. Radiocarbon 47, 57–65.

Hain, M.P., Sigman, D.M., Haug, G.H., 2011. Shortcomings of the isolated abyssal reservoir model for deglacial radiocarbon changes in the mid-depth Indo-Pacific Ocean. Geophys. Res. Lett. 38, L04604.

Hanslik, D., Jakobsson, M., Backman, J., Björck, S., Sellén, E., O'Regana, M., Fornaciaric, E., Skog, G., 2010. Quaternary Arctic Ocean sea ice variations and radiocarbon reservoir age corrections. Quat. Sci. Rev. 29, 3430–3441.

Heaton, T.J., Blackwell, P.G., Buck, C.E., 2009. A Bayesian approach to the estimation of radiocarbon calibration curves: The IntCal09 methodology. Radiocarbon 51, 1151–1164.

Hughen, K.A., Southon, J.R., Bertrand, C.J.H., Frantz, B., Zermeño, P., 2004. Cariaco Basin calibration update: revisions to calendar and ^{14}C chronologies for core PL07-58PC. Radiocarbon 46, 1161–1187.

Hughen, K.A., Southon, J., Lehman, S., Bertrand, C., Turnbull, J., 2006. Marine-derived ^{14}C calibration and activity record for the past 50,000 years updated from the Cariaco Basin. Quat. Sci. Rev. 25, 3216–3227.

Key, R.M., Kozyr, A., Sabine, C.L., Lee, K., Wanninkhof, R., Bullister, J.L., Feely, R.A., Millero, F.J., Mordy, C., Peng, T.-H., 2004. A global ocean carbon climatology: Results from GLODAP. Global Biogeochem. Cycles 18, GB4031.

Knorr, G., Lohmann, G., 2007. Rapid transitions in the Atlantic thermohaline circulation triggered by global warming and meltwater during the last deglaciation. Geochem. Geophys. Geosyst. 8, Q12006.

Köhler, P., Fischer, H., Munhoven, G., Zeebe, R.E., 2005. Quantitative interpretation of atmospheric carbon records over the last glacial termination. Global Biogeochem. Cycles 19, GB4020.

Kromer, B., Friedrich, M., Hughen, K.A., Kaiser, F., Remmele, S., Schaub, M., Talamo, S., 2004. Late glacial ^{14}C ages from a floating, 1382-ring pine chronology. Radiocarbon 46, 1203–1209.

Lohmann, G., 1998. The influence of a near-bottom transport parameterization on the sensitivity of the thermohaline circulation. J. Phys. Oceanogr. 28, 2095–2103.

Lohmann, G., Lorenz, S., 2000. On the hydrological cycle under paleoclimatic conditions as derived from AGCM simulations. J. Geophys. Res. 105, 417–436.

Lynch-Stieglitz, J., Adkins, J.F., Curry, W.B., Dokken, T., Hall, I.R., Herguera, J.C., Hirschi, J.J.-M., Ivanova, E.V., Kissel, C., Marchal, O., Marchitto, T.M., McCave, I.N., McManus, J.F., Mulitza, S., Ninnemann, U., Peeters, F., Yu, E.-F., Zahn, R., 2007. Atlantic Meridional Overturning Circulation During the Last Glacial Maximum. Science 316, 66–69.

Magana, A.-L., Southon, J.R., Kennett, J.P., Roark, E.B., Sarnthein, M., Stott, L.D., 2010. Resolving the cause of large differences between deglacial benthic foraminifera radiocarbon measurements in Santa Barbara Basin. Paleoceanography 25, PA4102.

Maier-Reimer, E., Mikolajewicz, U., Hasselmann, K., 1993. Mean circulation of the Hamburg LSG OGCM and its sensitivity to the thermohaline surface forcing. J. Phys. Oceanogr. 23, 731–757.

Mangini, A., Godoy, J.M., Godoy, M.L., Kowsmann, R., Santos, G.M., Ruckelshausen, M., Schroeder-Ritzrau, A., Wacker, L., 2010. Deep sea corals off Brazil verify a poorly ventilated Southern Pacific Ocean during H2, H1 and the Younger Dryas. Earth Planet. Sci. Lett. 293, 269–276.

Marchitto, T.M., Lehman, S.J., Ortiz, J.D., Fluckiger, J., van Geen, A., 2007. Marine radiocarbon evidence for the mechanism of deglacial atmospheric CO_2 rise. Science 316, 1456–1459.

McManus, J.F., Francois, R., Gherardi, J.-M., Keigwin, L.D., Brown-Leger, S., 2004. Collapse and rapid resumption of Atlantic meridional circulation linked to deglacial climate changes. Nature 428, 834–837.

Meland, M.Y., Dokken, T.M., Jansen, e., Hevrøy, K., 2008. Water mass properties and exchange between the Nordic seas and the northern North Atlantic during the period 23–6 ka: Benthic oxygen isotopic evidence. Paleoceanography 23, PA1210.

Monnin, E., Indermühle, A., Dällenbach, A., Flückiger, J., Stauffer, B., Stocker, T.F., Raynaud, D., Barnola, J.-M., 2001. Atmospheric CO_2 concentrations over the last glacial termination. Science 291, 112–114.

Muller-Karger, F., Varela, R., Thunell, R., Astor, Y., Zhang, H., Luerssenm, R., Hu, C., 2004. Processes of coastal upwelling and carbon flux in the Cariaco Basin. Deep Sea Res. II 51, 927–943.

Orr, J.C., Maier-Reimer, E., Mikolajewicz, U., Monfray, P., Sarmiento, J.L., Toggweiler, J.R., Taylor, N.K., Palmer, J., Gruber, N., Sabine, C.L., Le Quéré, C., Key, R.M., Boutin, J., 2001. Estimates of anthropogenic carbon uptake from four three-dimensional global ocean models. Global Biogeochem. Cycles 15, 43–60.

Otto-Bliesner, B.L., Hewitt, C.D., Marchitto, T.M., Brady, E., Abe-Ouchi, A., Crucifix, M., Murakami, S., Weber, S.L., 2007. Last Glacial Maximum ocean thermohaline circulation: PMIP2 model intercomparison and data constraints. Geophys. Res. Lett. 34, L12706.

Paul, A., Schäfer-Neth, C., 2003. Modeling the water masses of the Atlantic Ocean at the Last Glacial Maximum. Paleoceanography 18, 1058.

Peacock, S., 2010. Comment on "Glacial-interglacial circulation changes inferred from ^{231}Pa/^{230}Th sedimentary record in the North Atlantic region" by J.-M. Gherardi et al. Paleoceanography 25, PA2206.

Prange, M., Lohmann, G., Paul, A., 2003. Influence of vertical mixing on the thermohaline hysteresis: analyses of an OGCM. J. Phys. Oceanogr. 23, 731–757.

Prange, M., Lohmann, G., Romanova, V., Butzin, M., 2004. Modelling tempo-spatial signatures of Heinrich Events: Influence of the climatic background state. Quat. Sci. Rev. 23, 521–527.

Reimer, P.J., Baillie, M.G.L., Bard, E., Bayliss, A., Beck, J.W., Blackwell, P.G., Bronk Ramsey, C., Buck, C.E., Burr, G.S., Edwards, R.L., Friedrich, M., Grootes, P.M., Guilderson, T.P., Hajdas, I., Heaton, T.J., Hogg, A.G., Hughen, K.A., Kaiser, K.F., Kromer, B., McCormac, F.G., Manning, S.W., Reimer, R.W., Richards, D.A., Southon, J.R., Talamo, S., Turney, C.S.M., van der Plicht, J., Weyhenmeyer, C.E., 2009. IntCal09 and Marine09 radiocarbon age calibration curves, 0–50,000 years cal BP. Radiocarbon 51, 1111–1150.

Ritz, S.P., Stocker, T.F., Müller, S.A., 2008. Modeling the effect of abrupt ocean circulation change on marine reservoir age. Earth Planet. Sci. Lett. 268, 202–211.

Rose, K.A., Sikes, E., Guilderson, T.P., Shane, P., Hill, T.M., Zahn, R., Spero, H., 2010. Upper-ocean-to-atmosphere radiocarbon offsets imply fast deglacial carbon dioxide release. Science 446, 1093–1097.

Sarnthein, M., Gersonde, R., Niebler, S., Pflaumann, U., Spielhagen, R., Thiede, J., Wefer, G., Weinelt, M., 2003. Overview of Glacial Atlantic Ocean Mapping (GLAMAP 2000). Paleoceanography 18, 1030.

Sarnthein, M., Grootes, P.M., Kennett, J.P., Nadeau, M.-J., 2007. ^{14}C reservoir ages show deglacial changes in ocean currents and carbon cycle. In: Schmittner, A., Chiang, J., Hemmings, S. (Eds.), Ocean circulation: Mechanisms and impacts. American Geophysical Union Geophysical Monograph Series, Washington, D.C., pp. 175–196.

Schäfer-Neth, C., Paul, A., 2001. Circulation of the glacial Atlantic: a synthesis of global and regional modeling. In: Schäfer, P., Ritzrau, W., Schlüter, M., Thiede, J. (Eds.), The northern North Atlantic: A changing environment. Springer, Berlin, pp. 446–462.

Shin, S.-I., Liu, Z., Otto-Bliesner, B.L., Kutzbach, J.E., Vavrus, S.J., 2003. Southern Ocean sea-ice control of the glacial North Atlantic thermohaline circulation. Geophys. Res. Lett. 30, 1096.

Siegenthaler, U., Joos, F., 1992. Use of a simple model for studying oceanic tracer distributions and the global carbon cycle. Tellus 44B, 186–207.

Singarayer, J., Richards, D.A., Ridgwell, A., Valdes, P.J., Austin, W.E.N., Beck, J.W., 2008. An oceanic origin for the increase of atmospheric radiocarbon during the Younger Dryas. Geophys. Res. Lett. 35, L14707.

Sortor, R.N., Lund, D.C., 2011. No evidence for a deglacial intermediate water Δ^{14}C anomaly in the SW Atlantic. Earth Planet. Sci. Lett. 310, 65–72.

Stott, L., Southon, J., Timmermann, A., Koutavas, A., 2009. Radiocarbon age anomaly at intermediate water depth in the Pacific Ocean during the last deglaciation. Paleoceanography 24, PA2223.

Sweeney, C., Gloor, E., Jacobson, A.R., Key, R.M., McKinley, G., Sarmiento, J.L., Wanninkhof, R., 2007. Constraining global air-sea gas exchange for CO_2 with recent bomb ^{14}C measurements. Global Biogeochem. Cycles 21, GB2015.

Thornalley, D.J.R., Barker, S., Broecker, W.S., Elderfield, H.I., McCave, I.N., 2011. The deglacial evolution of North Atlantic deep convection. Science 331, 202–205.

Toggweiler, J.R., Dixon, K., Bryan, K., 1989. Simulations in a coarse-resolution world ocean model, 1. Steady state prebomb distributions. J. Geophys. Res. 94, 8217–8242.

Wunsch, C., Heimbach, P., 2007. Practical global oceanic state information. Physica D 230, 197–208.

Supplementary material to
Readjustment of glacial radiocarbon chronologies by
self-consistent three-dimensional ocean circulation modeling

by Martin Butzin, Matthias Prange and Gerrit Lohmann

Update of previous radiocarbon simulations

In this study we employ an updated relationship between wind speed and gas transfer velocity for $^{14}CO_2$ air-sea exchange following Sweeney et al. (2007). Compared to our previous study (Butzin et al., 2005) which followed Wanninkhof (1992), the $^{14}CO_2$ transfer velocity is about 33% lower in the global average. This leads to systematically higher radiocarbon ages in the simulations and improves the overall agreement with observations, as can be seen in Figures S-1 and S-2 which show model results for the preindustrial ocean obtained by the control run. The global-mean MRA (averaged over ice-free areas) is 540 a, which comes close to the values that can be derived from gridded GLODAP data (570 a; Key et al., 2004) and from scattered pre-bomb observations (Hughen et al., 2004; Guilderson et al., 2005; for comparison, the global-mean MRA according to Butzin et al., 2005 was 370 a). A simulation for the LGM (scenario GS discussed in Section 3.1) yields MRAs which are up to 2500 years higher than in the preindustrial ocean (shown in Fig. S-3).
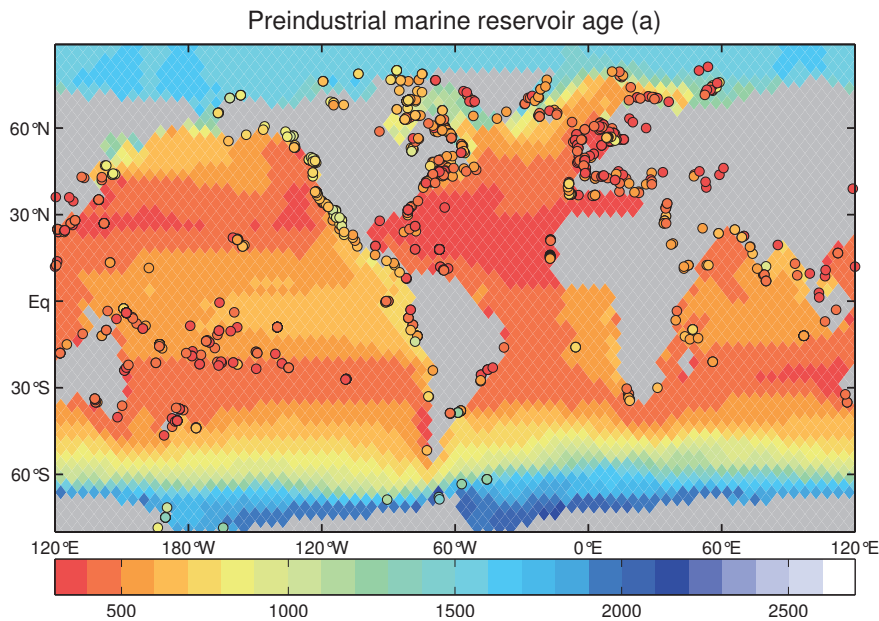

Fig. S1. Simulated marine reservoir age of the preindustrial ocean, shown are results of a control integration with present-day climate forcing (i.e. MOC scenario PD), atmospheric $\Delta^{14}C = 0\%_0$ and atmospheric $CO_2 = 280$ ppmv. Also shown are reconstructions derived from prenuclear marine samples collected in the Marine Reservoir Correction database (http://calib.qub.ac.uk/marine/; see http://calib.qub.ac.uk/marine/references.html for references).
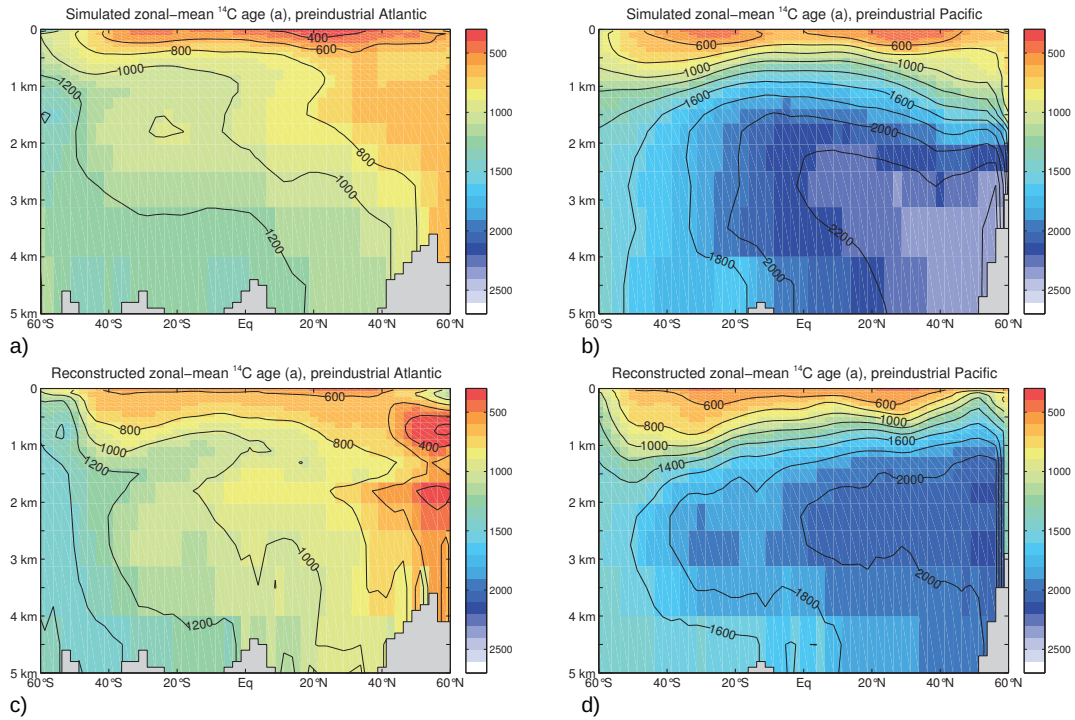
Fig. S2. Zonal-mean ^{14}C ages in the preindustrial ocean, shown are simulations for the Atlantic (a) and the Pacific (b) obtained in a control integration with present-day climate forcing (i.e. MOC scenario PD), $\Delta^{14}C_{atm} = 0\text{‰}$ and atmospheric $CO_2 = 280$ ppmv. Also shown are reconstructions for the Atlantic (c) and the Pacific (d) by Key et al. (2004).
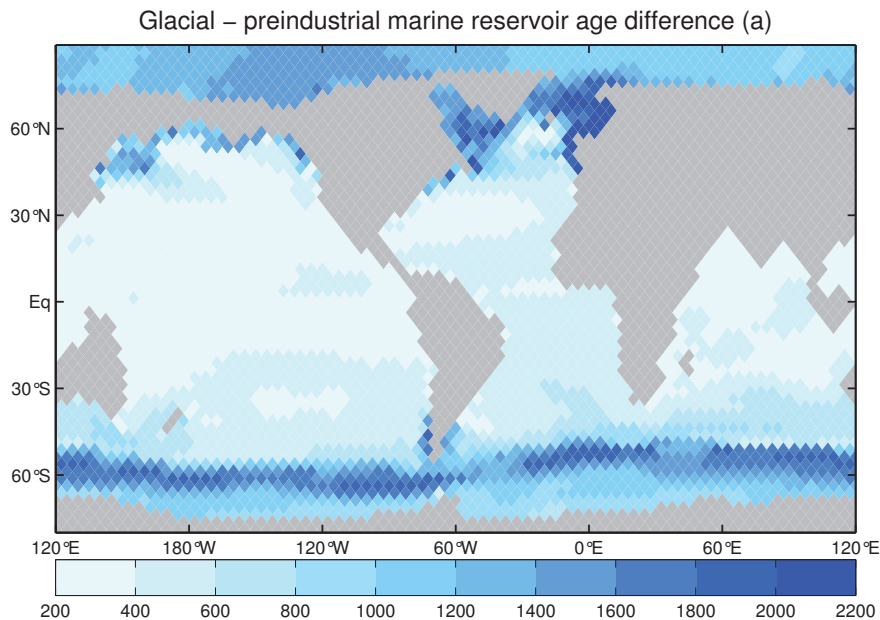

Fig. S3. Simulated marine reservoir age difference between the glacial ocean (according to the spinup with LGM climate forcing, i.e. MOC scenario GS, $\Delta^{14}C_{atm} = 520\text{‰}$ and atmospheric $CO_2 = 185$ ppmv) and the preindustrial ocean (control integration with present-day climate forcing, $\Delta^{14}C_{atm} = 0\text{‰}$ and atmospheric $CO_2 = 280$ ppmv).

A global estimate of ^{14}C fluxes

Combining marine and readjusted atmospheric ^{14}C histories it is possible to estimate deglacial air-sea ^{14}C fluxes. While there is no direct proxy for such fluxes, the estimates can be employed in ^{14}C budget considerations to verify the realism of our Δ^{14}C and MRA curves. For this purpose we consider the simplified global ^{14}C balance

$$P = \tfrac{d}{dt}{}^{14}\mathrm{C}_{atm} + \overline{k_{as}}\left({}^{14}\mathrm{C}_{atm} - \overline{{}^{14}\mathrm{C}_{mar}}\right) + \lambda\,{}^{14}\mathrm{C}_{atm} \qquad\qquad (A.1)$$

where $\tfrac{d}{dt}{}^{14}\mathrm{C}_{atm}$ denotes the temporal variation of atmospheric radiocarbon, $\overline{k_{as}}$ is the global-mean (but time-dependent) rate of air-sea exchange, and $\overline{{}^{14}\mathrm{C}_{mar}}$ is the global-mean radiocarbon concentration in surface water. The residual P can be interpreted as a crude estimate of cosmogenic ^{14}C production. Inserting model output fields of $^{14}\mathrm{C}_{atm}$, $\overline{{}^{14}\mathrm{C}_{mar}^{mod}}$ and $\overline{k_{as}}$ from the set of converged solutions, we arrive at radiocarbon fluxes of about 1.0–2.8 atoms cm^{-2} s^{-1}, which is in the lower range of reconstructions based on paleomagnetic and ice core records (e.g. Laj et al., 2002; Muscheler et al., 2004; Fig. S-4).
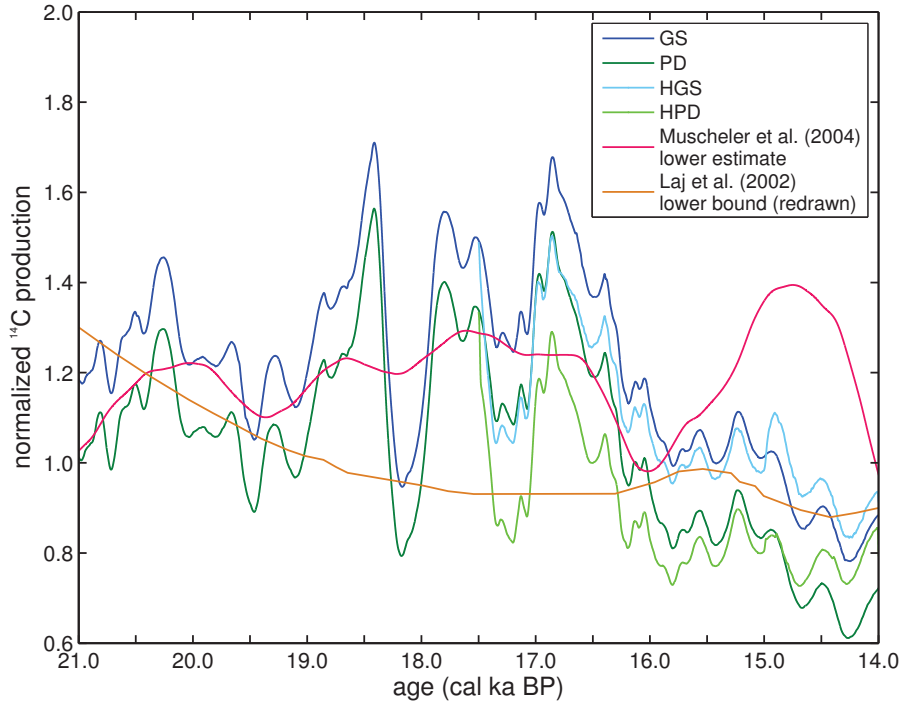

Fig. S4. Apparent cosmogenic ^{14}C production rates estimated from simplified global ^{14}C budget considerations. Also shown are lower bounds of reconstructions based on paleomagnetic records (redrawn from Laj et al., 2002) and ^{10}Be records (Muscheler et al., 2004). Values are normalized to the present-day flux (1.65 atoms cm^{-2} s^{-1} in the model runs).

References

Butzin, M., Prange, M., Lohmann, G., 2005. Radiocarbon simulations for the glacial ocean: The effects of wind stress, Southern Ocean sea ice and Heinrich events. Earth and Planetary Science Letters 235, 45–61.

Guilderson, T.P., Cole, J.E., Southon, J.R., 2005. Pre-bomb Δ^{14}C variability and the Suess effect in Cariaco Basin surface waters as recorded in hermatypic corals. Radiocarbon 47, 57–65.

Hughen, K.A., Southon, J.R., Bertrand, C.J.H., Frantz, B., Zermeño, P., 2004. Cariaco Basin calibration update: revisions to calendar and ^{14}C chronologies for core PL07-58PC. Radiocarbon 46, 1161–87.

Key, R.M., Kozyr, A., Sabine, C.L., Lee, K., Wanninkhof, R., Bullister, J.L., Feely, R.A., Millero, F.J., Mordy, C., Peng, T.-H., 2004. A global ocean carbon climatology: Results from GLODAP. Global Biogeochemical Cycles 18, GB4031.

Laj, C., Kissel, C., Mazaud, A., Michel, E., Muscheler, R., Beer, J., 2002. Geomagnetic field intensity, North Atlantic Deep Water circulation and atmospheric Δ^{14}C during the last 50 kyr. Earth and Planetary Science Letters 200, 177–190.

Muscheler, R., Beer J., Wagner, G., Laj, C., Kissel, C., Raisbeck, G.M., Yiou, F., Kubik, P.W., 2004. Changes in the carbon cycle during the last deglaciation as indicated by the comparison of ^{10}Be and ^{14}C records. Earth and Planetary Science Letters 6973, 1–16.

Sweeney, C., Gloor, E., Jacobson, A.R., Key, R.M., McKinley, G., Sarmiento, J.L., Wanninkhof, R., 2007. Constraining global air-sea gas exchange for CO_2 with recent bomb ^{14}C measurements. Global Biogeochemical Cycles 21, GB2015.

Wanninkhof, R., 1992, Relationship between wind-speed and gas- exchange over the ocean. Journal of Geophysical Research 97, 7373–7382.